JOURNAL OF SOLID STATE CHEMISTRY **123,** 150–160 (1996)
ARTICLE NO. 0163

The Structure of Fully H-Inserted γ-Manganese Dioxide Compounds

L. A. H. MacLean[1] and F. L. Tye

Energy Technology Centre, Middlesex University, Bounds Green Road, London N11 2NQ, United Kingdom

Received June 26, 1995; in revised form November 10, 1995; accepted January 22, 1996

Four materials forming a structural series of γ-manganese dioxides were identified by an increasing proportion of microtwinning (17–100%) and a nearly constant amount of de Wolff disorder ($P_r \simeq 0.41$) as determined from their XRD patterns. Chemical H-insertion was performed in a nonaqueous environment and the structure of the fully H-inserted compounds investigated by XRD. In contrast to the starting materials the H-inserted compounds had similar XRD patterns which could be indexed on the basis that H-insertion caused expansion predominantly in the *b* orthorhombic direction. The anisotropic expansion changed the angle of the 021 and 061 microtwinning planes and caused strain along them. The demicrotwinning which resulted was the reason for the similarity of the XRD patterns of the H-inserted compounds. The common endpoint of H-insertion into the structural series was δ-MnOOH, which is an unmicrotwinned intergrowth structure based on groutite and manganite type layers reflecting the original intergrowth of ramsdellite and pyrolusite type layers in the original host structures.

INTRODUCTION

Synthetic γ-manganese dioxides exhibit a wide range of differing crystal structures characterized mainly by their powder X-ray diffraction patterns (1). These range from a peak rich variety with some peaks showing selective broadening and shifts from the positions of orthorhombic ramsdellite to that of a typical commercial electrodeposited manganese dioxide (EMD) which normally displays only six broad peaks reflecting apparent hexagonal symmetry (2).[2] It is now well established that such materials act as host structures for H insertion (3–7). Although a new insight into the crystal structures of these host materials has emerged (see below), the nature of the H-inserted derivatives whether they are produced in a battery or by chemical insertion techniques has not been resolved. In order to investigate the structure of these H-inserted compounds H-insertion has been carried out on a range of γ-manganese dioxide materials which display related but differing X-ray diffraction patterns and form a structural series.

THE STRUCTURE OF γ-MANGANESE DIOXIDE

Pannetier *et al.* (2, 8–11) have succeeded in explaining the range of observed powder X-ray diffraction patterns with a new structural model which incorporates two types of crystal defects into an idealized ramsdellite host structure. The first type of defect (see Fig. 1) is a random planar fault based on the model originally constructed by de Wolff (12, 13) which exploits the fact that ramsdellite and pyrolusite (which are two of the known crystalline polymorphs of manganese dioxide (14)) possess intimately related structures due to the similarity of their oxygen frameworks. The pyrolusite (rutile) structure may be described as infinite single chains of edge sharing octahedra which are connected by corners to other single chains whereas the ramsdellite structure contains double chains. Figures 1a and 1b display idealized representations of these structures. In 1a the oxygens have primitive tetragonal packing (p.t.p.) (15) and in 1b the oxygens have an analogous packing arrangement based on a combination of body centred tetragonal packing (b.c.t.p.) (16) and hexagonal close packing (h.c.p.). The intergrowth structure represented in Fig. 1c may be described as a random distribution of ramsdellite layers R formed from double chains and r (rutile) layers formed from single chains. This type of random planar defect has been given the name de Wolff disorder (2).

The second type of defect is that of random microtwinning of the ramsdellite structure on the (021)/(061) planes. A full description of this type of fault, which also occurs in rutile (17), may be found in reference (11). Figure 2 displays this type of fault using a structural model shown in a recent paper (18) for the case of twinning on the 021 fault plane. It should be noted that the idealized oxygen packing arrangements described above are approximated to that of a h.c.p. in this model (and also in de Wolff's

[1] To whom correspondence should be addressed.

[2] Apparent hexagonal symmetry is strictly true only if the peak at approximately 4.1 Å is neglected.

0022-4596/96 $18.00

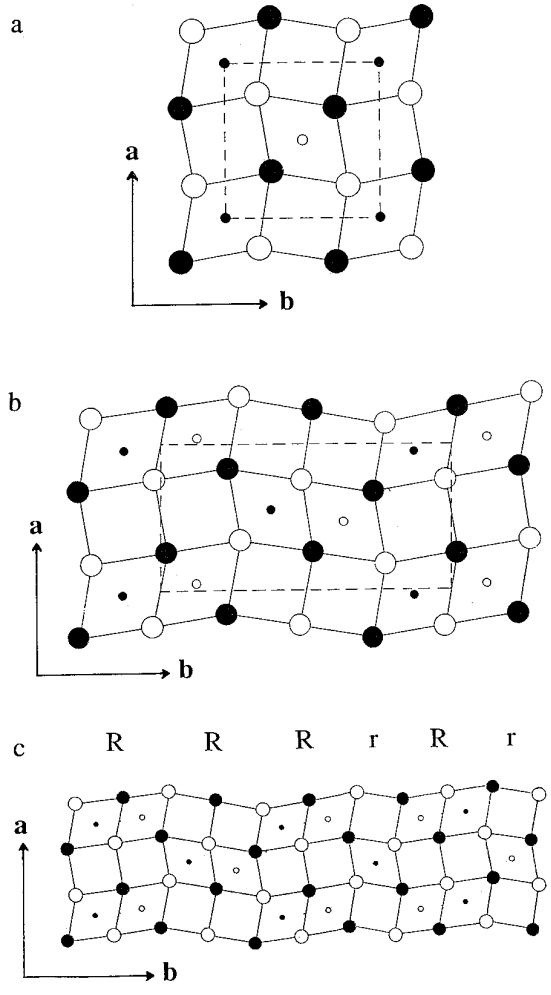

FIG. 1. (a) Idealized pyrolusite structure based on p.t.p. of oxygens. (b) Idealized ramsdellite structure based on a combination of b.c.t.p. and h.c.p. of oxygens. (c) A possible de Wolff intergrowth structure formed from a random sequence of layers derived from the structures shown in (a) and (b).

original model). Effectively microtwinning introduces a second type of random disorder this time in the *c* direction.

The results of this new structural model (which requires extensive numerical computation of the X-ray pattern) explains, *inter alia*, why the X-ray pattern of EMD possesses apparent hexagonal symmetry, the reason being that certain peaks in the X-ray diffraction pattern coalesce into combined peaks with increasing microtwinning faulting. In particular, peaks (221)/(240) and (061)/(002) coalesce into broad combined peaks as the microtwinning percentage approaches 100% (19).[3] This work for the first time investigates the structure of the fully H-inserted products starting from the above description introduced recently by Pannetier *et al.* for γ-manganese dioxide.

[3] It should be noted that the indices used in this work are not true miller indices since the structure contains random disorder in the *b* and *c* directions and thus no strictly periodic unit cell translations in those directions.

EXPERIMENTAL

Materials

Four manganese dioxides were studied: their structure covers the range of γ-manganese dioxide material described above. Starting with the line rich variety these are coded SBP-A (suspension bath process) (20), Faradiser WSZ from Sedema, International Battery Association (IBA) sample no. 14, and a commercial EMD coded R2 as in previous investigations (5, 6). The compositions (written as x in MnO_x and r in $MnOOH_r$ where $r = 4 - 2x$) of the materials are given in Table 1.

Preparation

The H-insertion compounds were prepared by reaction of the manganese dioxide with various chemical reductants

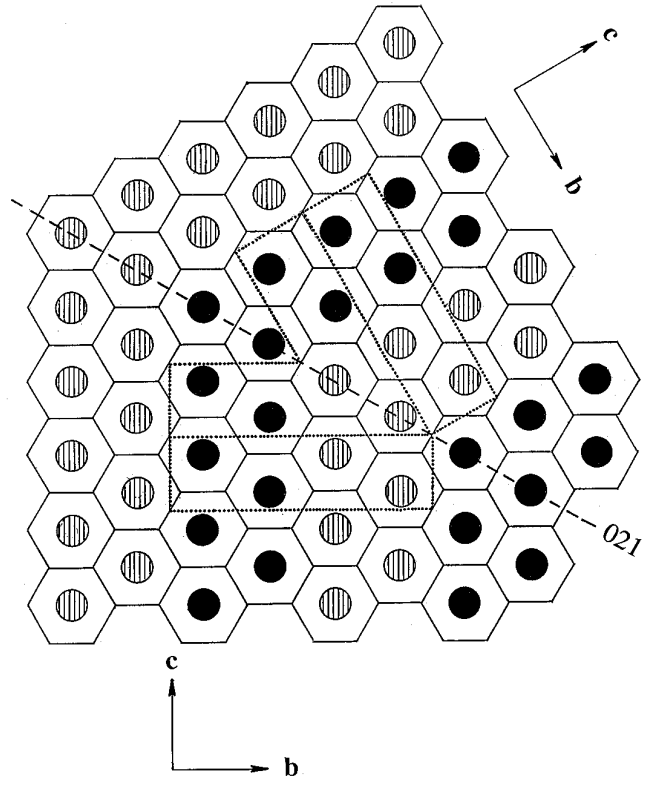

FIG. 2. Projection on the orthorhombic (*b*, *c*) plane of a possible microtwinning fault occurring in an idealized ramsdellite structure based on h.c.p. oxygens. Intersections show the position of oxygen atoms. Hatched and filled circles indicate Mn at $\frac{1}{4}$ and $\frac{3}{4}$ *a*. Ramsdellite double chain bends by 60° at the (021) fault line. The nonfaulted crystal has straight double chains extending in the *c* direction.

TABLE 1
Structural Parameters of the Materials

Material	x in MnO_x	r in $MnOOH_r$ ($r = 4 - 2x$)	Type	a_T	b_T	c_T	P_r	%Tw	Lines
Ramsdellite[a]	2.000[b]	0.000	I	4.533	9.27	2.866	0	0	All
SBP-A	1.966	0.068	I	4.442	9.33	2.849	0.41	17	S_1
WSZ	1.948[c]	0.104	I	4.462	9.38	2.844	0.38	27	S_1
IBA no. 14	1.957	0.086	II	4.418	9.47	2.846	0.41	≃50	S_2
R2	1.945[d]	0.110	III	a_{hex} 4.425	—	c_{hex} 4.440	0.43	≃100	S_2

Note. $S_1 \equiv$ The set of lines (021), (200), (121), (140), (221), (240), (002), and (061). $S_2 \equiv$ The set of lines (021), (200), (121), (221), (002), and (061).
[a] Lattice parameters from Byström (32).
[b] Ramsdellite is assumed to be a stoichiometric phase. From reference (31) for a sample of ramsdellite from Lake Valley, New Mexico (same location as Byström's sample) a value of $x = 2.00_6$ may be calculated.
[c] From reference (21).
[d] From reference (6).

in a nonaqueous environment. The techniques were chosen to minimize unwanted subsidiary chemical reactions in an attempt to produce as far as possible materials reflecting the fundamental solid state H-insertion process. H-insertion into material R2 has been described (6) and involved reaction of the manganese dioxide with combinations of cinnamyl alcohol, xylene, and acetone at room temperature. An essentially similar method using manganese dioxide in contact with either 1-propanol or 1-butanol under reflux was used to affect H-insertion of materials IBA no. 14 and SBP-A. Analar 1-propanol (99.5% pure, 0.2% water) dried with molecular sieve type 4A was used with quantities of manganese dioxide in which a 5 times excess of propanol was delivered estimated on the basis of Eq. [1], the likely reaction stoichiometry.

$$MnO_2 + CH_3CH_2CH_2OH \rightleftharpoons MnOOH + CH_3CH_2CH_2O \quad [1]$$

The top of the reflux tube was protected with silica gel to minimize water ingress over the reaction times required (56 h for IBA no. 14). Although 1-propanol proved a satisfactory reductant for IBA no. 14 full H-insertion was not achieved with SBP-A. A higher boiling alcohol (namely 1-butanol) was used in an attempt to produce a compound approaching full H-insertion (i.e., a compound with stoichiometry approaching MnOOH). With this material, which proved notably resistant to H-insertion, a compound with composition $MnOOH_{0.882}$ was achieved after 6 weeks of reflux. Longer reflux times tended to involve the formation of small quantities of Mn_2O_3 which was regarded as the product of a side reaction.

H-insertion into material WSZ was achieved with a new method using hydrazine hydrate suspended in hexane. Full details of the method may be found in reference (21). The fully H-inserted compounds produced by this method are known to have closely resembling X-ray diffraction patterns to those produced using the methods described above (22).

XRD Data Collection

A Philips PW 1700 XRD system was used employing Cu$K\alpha$ radiation, 1° divergence and scatter slits, 0.1 mm receiving slit, plus a graphite monochromator. Step scans were generally performed with $0.01°2\theta$ steps and a counting time of 1 s; a smoothing factor of 2 (as defined in the data collection software APD by Philips) was used in the presentation of the X-ray patterns. Samples of powdered manganese dioxide were ground for 3 min in a mortar and pestle and mounted by a backfilling procedure in flat aluminum holders. Peak positions were determined over three samples for materials R2 and IBA 14 and twice for materials SBP-A and WSZ (which have sharper peaks).

Chemical Analysis

Chemical analysis of the samples were performed to determine the level of H-insertion, in this case written as r in $MnOOH_r$ (23), by the double titration method of Vetter and Yeager (24) which enabled the available oxygen and total manganese to be determined on a single sample.

Structure Analysis

Analysis of the random nonperiodic layer structures of γ-manganese dioxide may be characterized by essentially two parameters, P_r, the probability of a rutile type layer, and %Tw, the % probability that a microtwin will occur. With %Tw = 0, $P_r = 0$ designates ramsdellite and $P_r = 1$ pyrolusite. The analysis for P_r and %Tw followed the method given by Pannetier (11, 19). It required unit cell refinement on the ''sharp lines'' which are unaffected by de Wolff disorder to find the apparent orthorhombic pa-

rameters, designated a_T, b_T, c_T. Since these depend on which lines are selected (11) (because microtwinning affects also the sharp lines) the lines used are indicated in Table 1. Calculation of %Tw is then possible by three methods, which are applicable to materials classified as type I or II (distinguished by the number of lines in the XRD patterns). These methods use the $b_T/2c_T$ ratio, the splitting of peaks (221)/(240), and the splitting of peaks (002)/(061). The value for %Tw listed in Table 1 followed closely the recommendations given by Pannetier. In the case of heavily microtwinned samples (type III) neither of the above methods is applicable to calculate %Tw since the pattern only contains six broad maxima (0°–70°2θ Cu$K\alpha$) due to convergence of the lines as mentioned previously. In this case %Tw is assumed to be close to 100% and the apparent hexagonal parameters are instead determined from the pattern. Calculation of P_r may then be carried out from the displacement of peak (110) from its orthorhombic position due to de Wolff disorder after correction for the shift due to microtwinning.

Table 1 shows that the concentration of de Wolff defects (P_r) is similar for all the materials studied whereas the %Tw fraction steadily increases in the direction SBP-A to R2. Essentially only one structural parameter varies which justifies the earlier assertion that the materials form a structural series.

RESULTS AND DISCUSSION

Figure 3 compares the X-ray patterns of the starting materials. They range from a line rich variety (Fig. 3a) to that of a typical EMD displaying only six broadened peaks in its X-ray pattern (pattern d, Fig. 3). The peaks in the pattern for SBP-A (Fig. 3a) divide into two classes following de Wolff. The so-called sharp lines which have $\frac{1}{2}k + l$ even (lines (021), (040), (200), (121), (140), (221), (240), (061), and (002), in the °2θ range 0–70 Cu$K\alpha$ radiation) and the broad lines (lines (110), (130), (111), (131) and (151) in the same °2θ range). As the sharp lines correspond to those lines unaffected by pyrolusite type (r) defaults, their positions relate to an orthorhombic cell of similar dimensions to that of the rare mineral ramsdellite. The remaining lines are both shifted and broadened from their orthorhombic position. The above description is only strictly true for materials which are free from microtwinning as this fault shifts and broadens all lines in the pattern. Table 1 indicates material SBP-A has a small microtwinning fraction and thus the description is approximately true for this material. For the other materials, however, all the lines are affected (Fig. 3b–3d) since they contain appreciable microtwinning fractions (see Table 1). Nevertheless values derived from the sharp lines are still useful parameters as outlined by Chabre and Pannetier (11). The lines used to calculate the apparent lattice parameters are

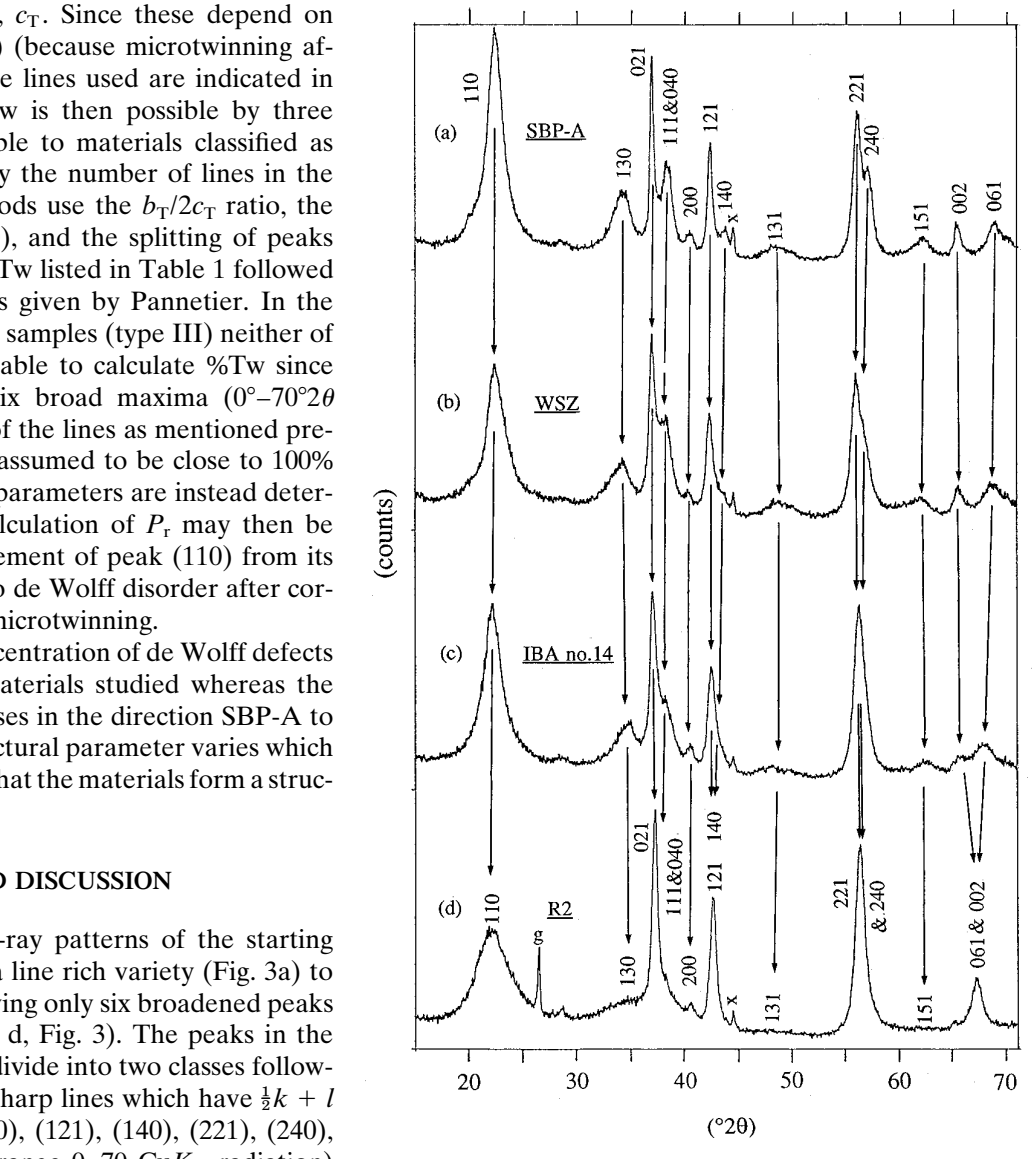

FIG. 3. Comparison of the powder X-ray diffractograms (Cu$K\alpha$ radiation) of (a) SBP-A, (b) WSZ, (c) IBA 14, and (d) R2. Orthorhombic indices related to those of ramsdellite are marked for (a). The arrows indicate the variation of position due to increasing microtwinning faulting (see also Table 1). The indices for (d) were ascertained from the progression in peak positions of the other members of the structural series (i.e., (a), (b), and (c)). x marks a peak from the sample holder, and g a graphite impurity peak.

indicated in Table 1. It is noted that the indices assigned to material R2 can be deduced from the progression of the series shown in Fig. 3, i.e., independently of any assumption concerning the nature of the fault which explains the series.

For the fully H-inserted materials a corresponding figure to Fig. 3 may be constructed and is shown in Fig. 4. Concentrating first on the X-ray diffractogram of H-inserted SBP-A it is seen to contain the same number of lines as

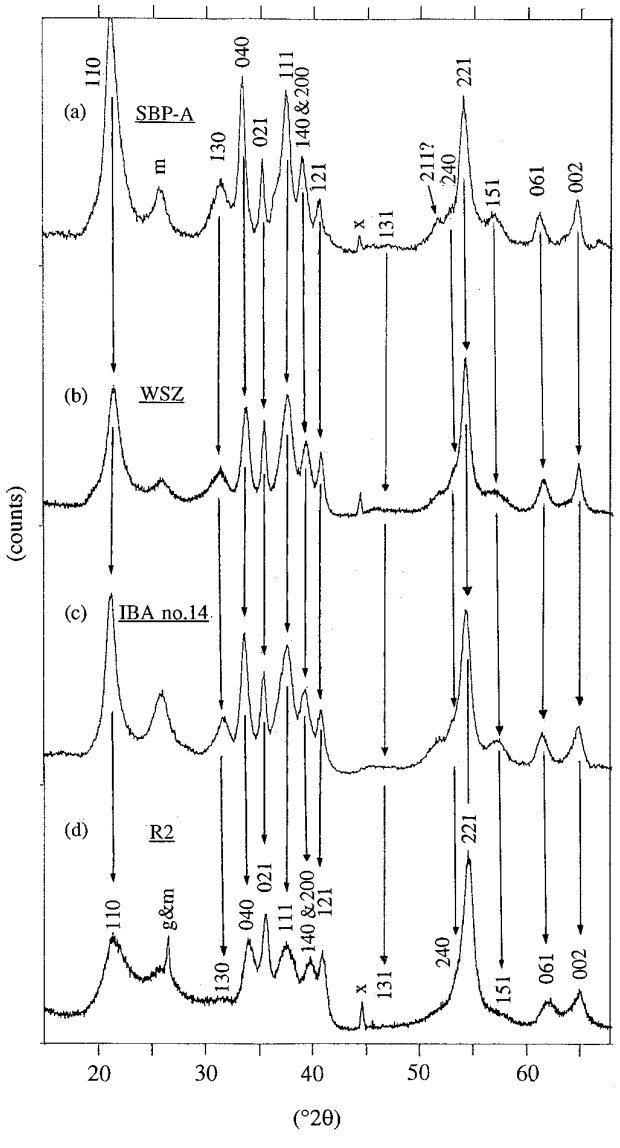

FIG. 4. Comparison of the powder X-ray diffractograms (Cu$K\alpha$ radiation) of the fully H-inserted manganese dioxides (a) SBP-A, (b) WSZ, (c) IBA 14, and (d) R2. Orthorhombic indices related to those of groutite are marked for the different H-inserted materials. Arrows connect peaks of the same indices. The indices for (d) were ascertained from following the arrows from (a), as for (d) in Fig. 3. g marks a graphite impurity peak and x a peak from the sample holder. m marks the 100% line in manganite.

the initial material. Figure 5 compares the XRD patterns of SBP-A and its most H-inserted derivative. If the peak marked m in Fig. 5 and the shoulder on (240) labeled (211) are neglected then every line in the starting material has a counterpart in the H-inserted material. It is considered that peak m represents a manganite impurity resulting from precipitation of the slightly soluble manganese in the organic solvent rather than a peak resulting from the fundamental H-insertion reaction. The remaining peaks in the H-inserted material may all be assigned indices which are related to those of groutite (which has the composition MnOOH) in the same way as the peaks in the starting material are related to ramsdellite. As groutite and ramsdellite belong to the same space group (*Pbnm*) and structure (25) it is tempting to link the common indices as shown in Fig. 5. The indices of the other H-inserted materials were assigned by comparison with this structure in an analogous fashion to that of the starting materials. Using these indices it was possible to determine unit cell parameters for the H-inserted materials in a similar way to that determined for the starting materials.

Table 2 indicates the lattice parameters and lines used to calculate these parameters for the most H-inserted materials. Also given are the levels of H-insertion for each material. The level of H-insertion is close to that of the theoretical limit MnOOH in all cases except that of material SBP-A. In this case, however, the H-insertion process was heterogeneous from a low level of H-insertion (r = 0.35) and therefore the product observed at higher levels was almost wholly characteristic of the most H-inserted product (26), particularly in regard to peak positions.

This analysis indicates that all the lines present in the starting materials are present in the most H-inserted derivatives with the exception of the manganite line (labeled m in Fig. 4). In Fig. 4 the arrows connect peaks of the same indices as in Fig. 3. Clearly the XRD patterns are similar in that they all contain the same number of peaks although some peaks in the material produced from the heavily microtwinned host (Fig. 4d) are very weak.

The appearance of the line labeled m (Figs. 4 and 5) is unconnected with the appearance of the other new lines which emerge with H-insertion. Figure 6 compares a compound prepared at low temperature (≈2°C) with one prepared at ambient temperature. The complete absence of the manganite peak in the low temperature compound but the obvious similarity of the remaining peaks (at similar H-insertion levels) confirms that this peak is due to a manganite impurity. Further examination of Fig. 6 reveals that the background level in the region of peak m is similar. The quantity of manganite in the compound was estimated by subtracting the pattern of the low temperature compound from the one produced at higher temperature to obtain the area under peak m. Comparison of the area under the peak to that of a pure manganite sample obtained from refluxing a fully H-inserted EMD sample in distilled water for 20 h revealed that 9% of manganite was present. A related procedure showed that H-inserted IBA no. 14 had 20% of manganite and the other compounds less than 11%. From previously published data on a set of R2 H-inserted samples by Fitzpatrick and Tye (6) of which the most H-inserted one is included in this work hardly any loss in intensity of the (110) peak in the composition

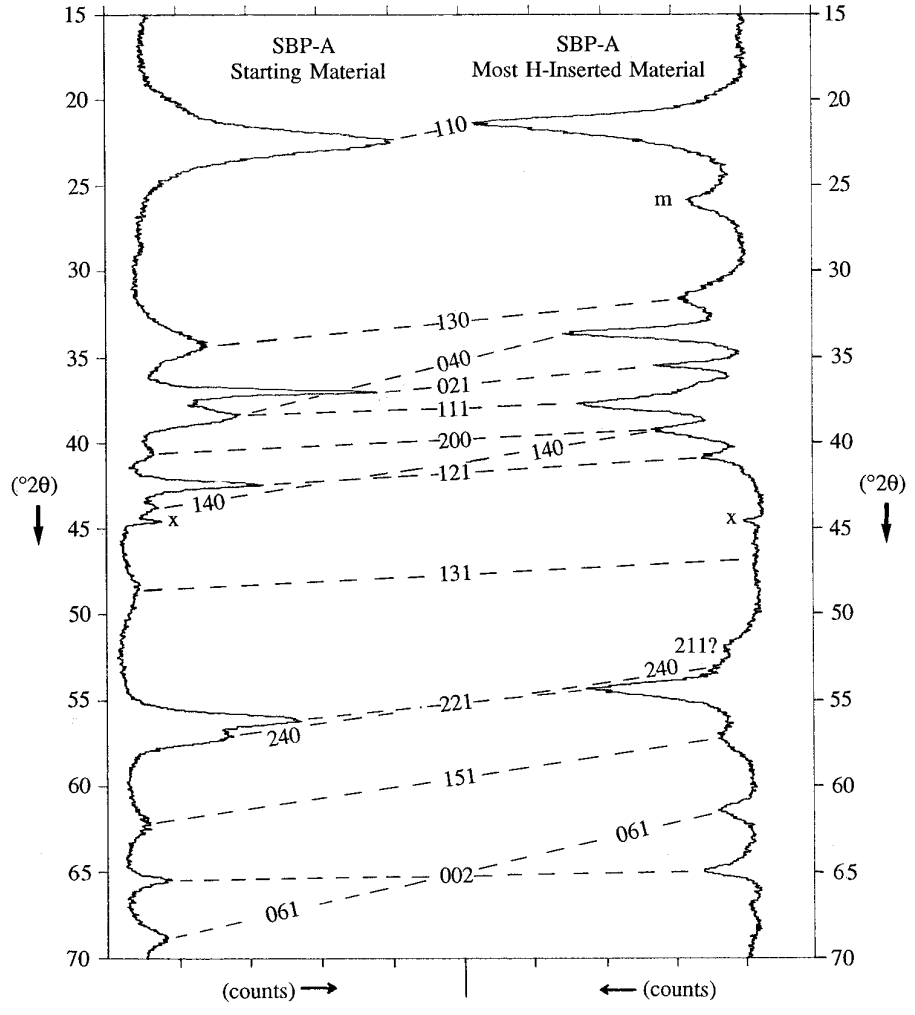

FIG. 5. Powder X-ray diffraction pattern (Cu$K\alpha$ radiation) comparison of material SBP-A and its most H-inserted derivative.

region $MnOOH_{0.80}$ to $MnOOH_{1.01}$ was observed which is consistent with the analysis of a low manganite content (see Fig. 4 of ref. (6)). Although the presence of manganite may bias positions of lines in the XRD patterns of the H-inserted products this is not considered to significantly affect the results because as shown in Fig. 6 samples with and without manganite were otherwise nearly identical.

Since each peak in the starting material is present in the H-inserted material (except the peak tentatively assigned (211) in Fig. 5) a graph of the expected shift of each line as determined from the expansion of the orthorhombic lattice and the measured shift of each line from the X-ray patterns may be constructed, the object being to discover whether all the peaks in the pattern (i.e., including the broad lines) are in the expected position as calculated from the expansion of the orthorhombic lattice (which is derived from the position of the lines given in Tables 1 and 2). If the structure of the most H-inserted compound is an expanded analog of the original material such a graph would produce a straight line. Figure 7 presents such a graph for material SBP-A. Since the lattice parameters were derived from the set of lines S_1 (see Table 1) those lines naturally fall close to the straight line which indicates that the measured and expected shifts are the same. The remaining (broad) lines (namely peaks (130), (110), (151), and (111)) also fall close to the straight line. Peak (131) is not shown since its breadth precluded accurate measurement particularly in the H-inserted compound. Peak (240) although visible in the starting material only occurs as weak shoulder on (221) in the fully H-inserted compound and is also excluded.

The results of the above procedure establish that H-inserted SBP-A material possesses an expanded version of the original structure. Table 2 indicates that the expansion is primarily in the *b* orthorhombic direction and is of similar dimensions to that expected from the hypothetical

TABLE 2
Structural Parameters of the H-Inserted Materials

H-inserted material	r in $MnOOH_r$	a	b	c	Lines
Groutite	1.00[a]	4.560 {0.60%}[b]	10.700 {15.43%}	2.870 {0.14%}	All
SBP-A	0.88	4.561 {2.68%}	10.64 {14.04%}	2.869 {0.70%}	S_3
WSZ	0.97[c]	4.542 {1.79%}	10.58 {12.80%}	2.869 {0.88%}	S_3
IBA no. 14	0.99	4.545 {2.87%}	10.61 {12.04%}	2.876 {1.05%}	S_3
R2	1.01[d]	4.514 {N/A}	10.49 {N/A}	2.867 {N/A}	S_3

Note. $S_3 \equiv$ The set of lines (021), (040), (200), (121), (140), (221), (002), and (061).

[a] Assumed to be stoichiometric. Lattice parameters from ref. (25).

[b] Percentage expansion of the a, b, or c lattice parameters compared to those of the starting materials given in Table 1.

[c] From reference (21).

[d] From reference (6).

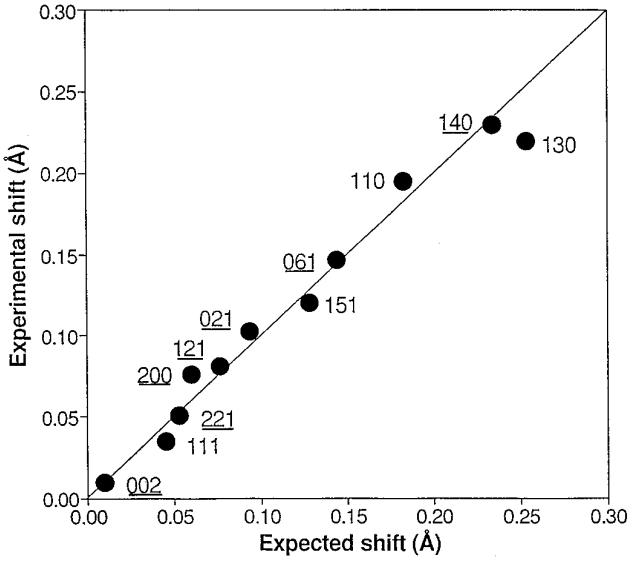

FIG. 7. Expected line shift versus measured line shift for materials SBP-A and its most H-inserted derivative. Underscored indices mark which peaks were used in the determination of the orthorhombic parameters.

transition ramsdellite to groutite. The most probable source of error from the straight line in Fig. 7 results from the determination of the lattice parameters from the sharp lines which are shifted (in differing directions) because of the effects of a small microtwinning percentage.

A similar procedure was used to establish that the materials resulting from H-insertion into WSZ and IBA 14 also are expanded analogs of their parent structures. The appearance of new or extra lines in heavily microtwinned H-inserted samples (compare Fig. 4d and Fig. 3d) is now clearly seen to be the result of anisotropic expansion of the structure such that lines previously overlapped in the starting material are now separated in the H-inserted product, as suspected by Fitzpatrick and Tye (6).

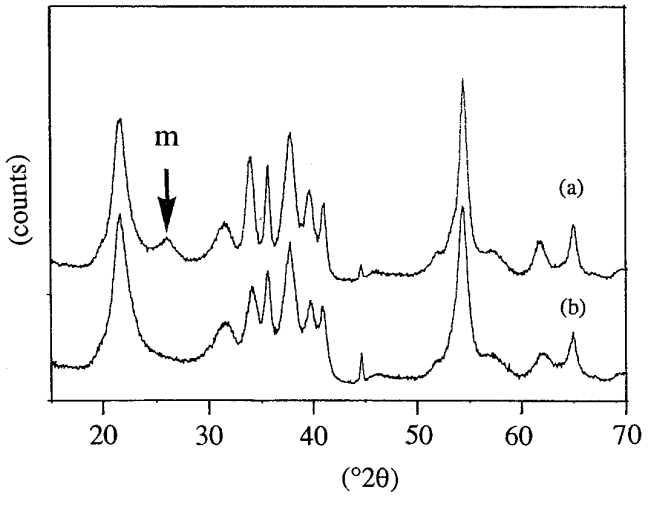

FIG. 6. XRD (Cu$K\alpha$ radiation) comparison of nonaqueous hydrazine H inserted WSZ. (a) Ambient temperature, $MnOOH_{0.958}$. (b) Low temperature (≈2°C), $MnOOH_{0.956}$. In (a) manganite formation is indicated by an arrow.

The magnitude of the expansion for the H-inserted samples SBP-A, WSZ, IBA no. 14, and R2 (apparently) decreases as the percentage of microtwinning increases such that the fully H-inserted structures all possess similar orthorhombic lattice parameters (Table 2). This suggests that the structures of the fully H-inserted materials are similar despite starting from different points in the structural series. Comparison of Fig. 3 showing the structural series formed by the starting materials and Fig. 4 supports this notion. For example, in Fig. 3 peaks 002/061 and 221/240 coalesce into single peaks as the percentage of microtwinning increases but no equivalent peak movement is apparent in the most H-inserted products (Fig. 4). In fact, the X-ray patterns of the most H-inserted materials all exhibit peaks in similar positions but of differing broadness and intensity. This in turn strongly suggests that the materials have lost the structural defect responsible for the series in the starting materials, namely microtwinning. If this hypothesis is correct the structures must have at some point in the H-insertion reaction undergone a change which causes demicrotwinning of the structure. Thus the percentage (given in brackets) lattice parameter expansions given in Table 2 are only apparent expansions since the end members are not affected by microtwinning whereas the initial lattice parameters are (Table 1). In the case of material SBP-A, however, the initial microtwinning fraction is

TABLE 3
Estimated Lattice Parameters of the Starting Materials from Their H-Inserted Derivatives

Material	*a*	*b*	*c*	*b*/2*c*	%Tw (after demicrotwinning)
WSZ	4.423	9.27	2.849	1.626	7
IBA no. 14	4.426	9.29	2.856	1.627	8
R2	4.401	9.19	2.847	1.614	−3

low (Table 1) and therefore the lattice parameter expansion is closest to the actual lattice parameter expansion. It is therefore possible to estimate the real or predominant starting lattice parameters for the remaining materials by contraction of the H-inserted lattice by the same amount as deduced for material SBP-A.[4] Table 3 contains the result of this procedure. If the final H-inserted materials were demicrotwinned recalculation of %Tw from the predominant lattice parameters should yield a result close to zero. The results shown in Table 3 calculated from the formula (11)

$$\%\mathrm{Tw} = 871(b/2c) - 1409 \qquad [2]$$

support the important conclusion that full H-insertion causes demicrotwinning.

It is noted that the lattice parameter expansion used in the above argument was that found for SBP-A and its most H-inserted derivative which was preferred to that predicted from the nonfaulted phases ramsdellite and groutite because ramsdellite is nearly perfectly stoichiometric (Table 1) whereas γ-MnO_2 is always nonstoichiometric (x in MnO_x (generally) ≤ 2)). Thus the lattice parameters for γ-MnO_x are not necessarily expected to be the same (even for a hypothetical γ-MnO_x material with %Tw = 0 and $P_r = 0$) as for ramsdellite especially if nonstoichiometry is due to Mn^{3+} in the structure.

FURTHER DISCUSSION

Giovanoli *et al.* (7) first concluded that the structure of an H-inserted compound synthesized by reduction with cinnamyl alcohol in xylene retained qualitatively similar line shifts to those expected from the de Wolff model of γ-MnO_2. That is to say the material possessed a random intergrowth structure of manganite type layers dispersed in a groutite-like framework structure. In this work, following Maskell *et al.* (5), this structure is given the name δ-MnOOH. The XRD trace of the material studied by Giovanoli *et al.* displays a remarkably similar pattern to that of the most H-inserted SBP-A. When the γ-MnO_2 was "extremely disperse," however, they claimed that γ-MnOOH was produced not δ-MnOOH in a double phase reaction. It is clear that what Giovanoli recognized as extremely disperse γ-MnO_2 is what he later regarded (27) as "ε-MnO_2" which corresponds to the material coded R2 in this work. The conclusion that γ-MnOOH is the structure of the most H-inserted product was later found to be tenable only when the reduction occurred in aqueous solution (5). Ozhuku and Hirai (28) who also studied a range of materials similar to the range studied in this work concluded that H-inserted EMD produced "mixed reduction products of groutite and manganite" in a "single phase" reduction and furthermore that the crystal structure of the products from the range of materials reflected the structures of the manganese dioxide used. Since an aqueous solution of hydrazine hydrate was used to effect the reduction the authors believe complicating side reactions (29) were not eliminated and the structures produced were not solely the result of the fundamental solid state H-insertion reaction.

In this work the results have been successfully interpreted on the basis that all the H-inserted products are essentially expanded analogs of their parent structures. The expansion was found to be anisotropic and directed with the greatest degree along the *b* orthorhombic direction for all the materials. In the case of SBP-A the relative expansion was close to that expected from the hypothetical transition ramsdellite to groutite as has already been pointed out. Material SBP-A, however, is not a perfectly crystalline phase as it possesses de Wolff disorder, i.e., randomly interspersed R and r type layers. The plausibility of the corresponding H-inserted intergrowth structure, namely randomly alternating G (groutite) and m (manganite) type layers or δ-MnOOH, is enhanced by noting the following structural relationship between the structures pyrolusite and manganite as given in Table 4. Compared to pyrolusite manganite contains oxygen atoms which are not equivalent such that the structure in the *a* and *c* direc-

TABLE 4
Unit Cell Comparison between Pyrolusite and Manganite

Material	*a*	*b*	*c*	Unit cell type	Reference
Pyrolusite	4.40	4.40	2.87	tetragonal	32
(Manganite)	(8.86)	(5.24)	(5.70)	(monoclinic)	30
Unit cell derived from manganite	4.43	5.24	2.85	N/A	
% increase	0.68%	19.09%	−0.70%		

[4] Even in the case of materials with %Tw = 0 de Wolff disorder may still be present which means that the lattice parameters derived from the sharp lines reflect the predominant R lattice.

tions becomes (approximately) doubled. Division of the *a* and *c* axis by two produces a unit cell which can be compared to pyrolusite; see Table 4. This procedure indicates, as in the case for ramsdellite to groutite, that the expansion is anisotropic and directed along the equivalent of the *b* orthorhombic direction. The magnitude of the change is 19% as compared to 15% for ramsdellite to groutite with less than a 1% change in the other two directions (as is the case for ramsdellite to groutite, see Table 2). Figure 8 represents the relationship between pyrolusite and manganite and also ramsdellite and groutite by superimposing unit cells. Thus, on this basis, if an intergrowth structure of R and r type layers is plausible so is the corresponding H-inserted intergrowth structure of G and m type layers.

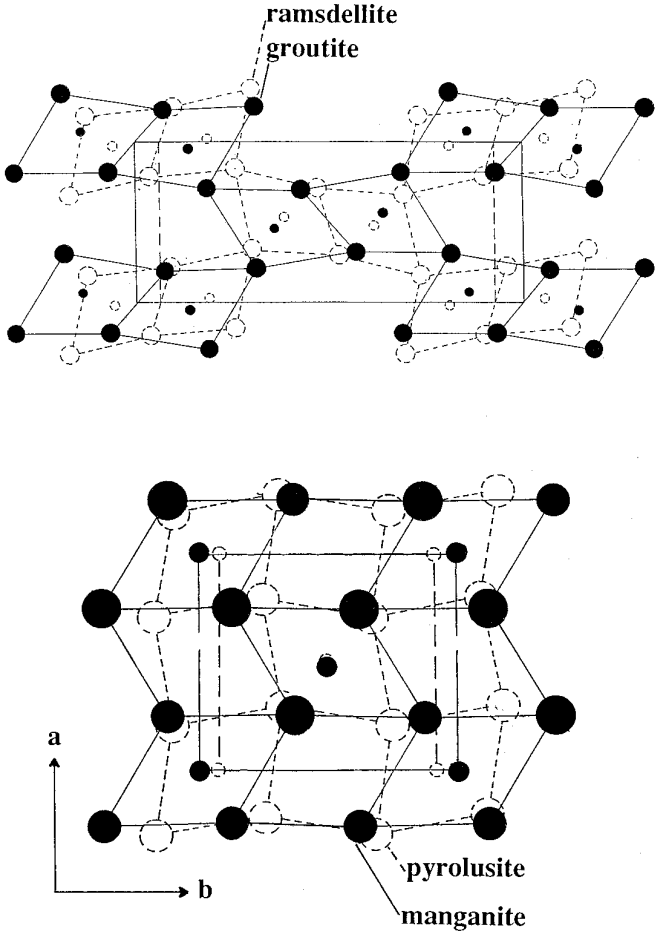

FIG. 8. (a) Superimposed unit cells of groutite and ramsdellite showing the relation between the structures. *a* appears coincident in both drawings whereas *b* is 15% larger in groutite. *c* (perpendicular to the plane of the drawing) is also nearly equal for both structures (Table 2). (b) Similar comparison between manganite and pyrolusite. In this case half a unit cell (in the *a* and *c* directions) was used for manganite. The *a* and *c* unit cell parameters are again nearly equal whereas *b* is 19% greater in manganite (Table 2).

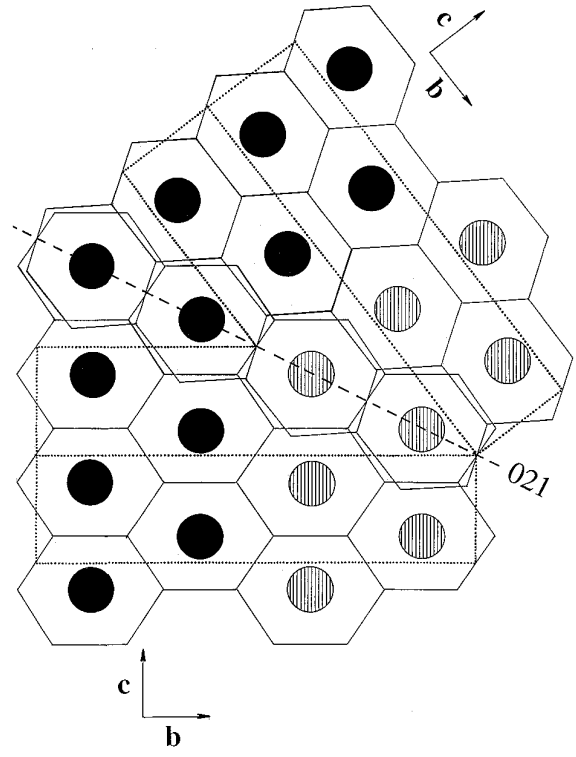

FIG. 9. Demonstration of the incompatibility between anisotropic expansion and microtwinning. Projection on the *bc* plane of superimposed expanded ramsdellite structure at a 021 microtwin boundary. The idealized octahedra (shown in Fig. 2) are expanded by 19% in the *b* direction. Oxygen mismatch is evident leading to strain at the boundary.

Origin of Demicrotwinning

The notion of demicrotwinning[5] may be understood by considering what happens to a region of the crystal which is microtwinned when H is inserted. In this case, as in the case of the hypothetical transition between ramsdellite and groutite, the structure expands primarily in the *b* orthorhombic direction. A consequence of anisotropic expansion of the structure is a change in strain across the microtwinning fault planes. Figure 9 demonstrates this point by superimposing anisotropically expanded structures of idealized microtwinned ramsdellite projected on the *bc* plane in the region of the twin boundary (compare with Fig. 2). In this representation the 021 fault line was chosen to be common to structures based on octahedra expanded by 19% in the *b* orthorhombic direction at each side of the twin boundary. Since the structures must be the same on both sides of the fault line a mismatch in the oxygen positions is evidently induced at the boundary. Oxygens on

[5] The origin of demicrotwinning in this case should be clearly distinguished from the proposed "detwinning" of γ-MnO_2 during heat treatment introduced by Ripert *et al.* (10) to account for the observed decrease of the $b/2c$ ratio from NPD measurements.

either side of the 021 plane must therefore occupy compromise positions which have less stability than corresponding positions in an unmicrotwinned structure. The microtwinning planes are therefore planes of weakness. The expansion in the *b* direction also causes a change in the angle between the microtwinning plane and the *b* or *c* directions. In a polycrystalline entity this angle change generates the forces which cause splitting along the planes of weakness, in other words demicrotwinning. Similar arguments apply to microtwinning where 061 is the fault plane. The presence of de Wolff faults in the ramsdellite structure also does not alter the argument. This explains why the fully H-inserted materials possess similar *X*-ray diffraction patterns since they all contain similar concentrations of de Wolff faults (Table 1). The differing peak intensities and breadth now may be seen to result from a differing degree of break up of the structures into finer crystallites sizes. Thus as expected, fully H-inserted SBP-A produces the X-ray pattern with the sharpest and most intense lines whereas H inserted R2 produces a material with broad less intense peaks. Examination of the powders by SEM, however, revealed no obvious breakup of the particles whose shape apparently remained unaltered before and after H-insertion. It must be supposed therefore that strains induced are sufficiently strong to present smaller crystallites for X-ray diffraction without causing breakup of individual particles.

The above interpretation implies that the correct description of the structure of all the fully H-inserted end products formed by the fundamental solid state H-insertion reaction from the structural series of γ-manganese dioxides studied is that of δ-MnOOH as proposed by Maskell *et al.* (5), i.e., a random alternation of groutite G and manganite type m building layers similar to the original description of γ-MnO_2, namely a random alternation of ramsdellite R and pyrolusite (rutile) r type layers as first formulated by de Wolff.

CONCLUSIONS

1. The product from a nonaqueous H-insertion reaction into a range of γ-manganese dioxide has a structure which retains the same space group and structure type as the host material but with a unit cell expanded predominantly in the *b* orthorhombic direction.

2. H-insertion into a low microtwinned γ-manganese dioxide produced a material in which each peak had a corresponding peak in the H-inserted counterpart with the same *hkl* indices.

3. The contrast between the similarity of the XRD patterns of the H-inserted material and their dissimilarity in the starting material indicated strongly that H-insertion caused demicrotwinning.

4. The position of additional peaks after H-insertion into heavily microtwinned host material are believed to be a result of both demicrotwinning and anisotropic expansion in the *b* orthorhombic direction.

5. The common H-inserted product from materials having a range of microtwinning but nearly constant de Wolff disorder is δ-MnOOH, which is an unmicrotwinned intergrowth structure having a random alternation of groutite type and manganite type layers.

ACKNOWLEDGMENTS

The authors acknowledge the contributions of J. Fitzpatrick and J. Larcin who, respectively, prepared and chemically analyzed the H-inserted R2 and WSZ samples. We also thank E. Preisler who kindly supplied the material prepared by the suspension bath process coded SBP-A in this work. One of the authors (L.A.H.M.) also thanks J. Pannetier for many stimulating discussions on the subject of microtwinning.

REFERENCES

1. D. G. Malpas and F. L. Tye, *in* "Handbook of Manganese Dioxides Battery Grade" (D. Glover, B. Schumm Jr., and A. Kozawa, Eds.), Chap. 5. I.B.A. Inc., 1989.
2. J. Pannetier, *Prog. Batteries Battery Mater.* **11,** 51 (1992).
3. W. Feitknecht, H. R. Oswald, and V. Feitknect-Steinmann, *Helv. Chim. Acta.* **43,** 1947 (1960).
4. J. P. Gabano, B. Morignat, E. Fialdes, B. Emery, and J. F. Laurent, *Z. Phys. Chem.* **46,** 359 (1965).
5. W. C. Maskell, J. E. A. Shaw, and F. L. Tye, *Electrochim. Acta.* **26,** 1403 (1981).
6. J. Fitzpatrick and F. L. Tye, *J. Appl. Electrochem.* **21,** 130 (1991).
7. R. Giovanoli, K. Bernhard, and W. Feitknecht, *Helv. Chim. Acta.* **52,** 2333 (1969).
8. J. Pannetier, Y. Chabre, and C. Poinsignon, *ISSI Lett.* **1**(2), 5 (1990).
9. M. Ripert, C. Poinsignon, Y. Chabre, and J. Pannetier, *Phase Trans.* **32,** 205 (1991).
10. M. Ripert, J. Pannetier, Y. Chabre, and C. Poinsignon, *Mat. Res. Soc. Symp. Proc.* **10,** 359 (1991).
11. Y. Chabre and J. Pannetier, *Prog. Solid State Chem.* **23,** 1 (1995).
12. P. M. de Wolff, *Acta Crystallogr.* **12,** 341 (1959).
13. J. H. A. Laudy and P. M. de Wolff, *Appl. Sci. Res. Sect. B,* **10,** 157 (1963).
14. A. F. Wells, "Structural Inorganic Chemistry," 5th ed., p. 553. OUP, 1984.
15. A. R. West and P. G. Bruce, *Acta Crystallogr. B* **38,** 1891 (1982).
16. W. I. F. David, P. G. Bruce, and J. B. Goodenough, *J. Solid State Chem.* **50,** 235 (1983).
17. K. Suzuki, M. Ichihara, and S. Takeuchi, *Phil. Mag. A* **63,** 657 (1991).
18. F. L. Tye, and S. W. Tye, *J. Appl. Electrochem.* **25,** 425 (1995).
19. J. Pannetier, *Prog. Batteries Battery Mater.* **13,** 132 (1994).
20. E. Preisler, *J. Appl. Electrochim.* **19,** 540 (1989).
21. J. Larcin, "Chemical and Electrochemical Studies of Leclanché Cells." Ph.D. Thesis, 1991.
22. J. Jones, W. C. Maskell, and F. L. Tye, unpublished.
23. S. Atlung, "Manganese Dioxide Symposium" (A. Kozawa and R. J. Brodd, Eds.), Vol. 1, Cleveland, 1975.
24. K. J. Vetter and N. Yeager, *Electrochim. Acta.* **11,** 401 (1966).
25. L. S. Dent Glasser and Lorna Ingram, *Acta Crystallogr. B* **24,** 1233 (1968).
26. L. A. H. MacLean and F. L. Tye, in preparation.

27. R. Giovanoli, ''Manganese Dioxide Symposium'' (B. Schumm Jr., H. M. Joseph, and A. Kozawa, Eds.), Vol. 2. Tokyo, 1980.
28. T. Ohzuku and T. Hirai, ''Manganese Dioxide Electrode Theory and Practice for Electrochemical Applications'' (B. Schumm, R. L. Middaugh, M. P. Grotheer, and J. C. Hunter, Eds.), p. 141–157. The Electrochem. Soc. Inc., 1985.
29. D. M. Holton, W. C. Maskell, and F. L. Tye, ''Power Sources 10'' (L. Pearce, Ed.), p. 247. The Paul Press, London, 1985.
30. M. J. Buerger, *Zeit. Kristallogr.* **95,** 163 (1936).
31. M. Fleischer, W. E. Richmond, and H. T. Evans Jr., *Amer. Miner.* **47,** 47 (1962).
32. A. M. Byström, *Acta Chem. Scand.* **3,** 163 (1949).